Electronic Supplementary Material (ESI) for Journal of Materials Chemistry A.

Electronic Supplementary Material

Developing intercalation based anode materials for fluoride-ion batteries: Topochemical reduction of $Sr_2TiO_3F_2$ via a hydride based defluorination process

Kerstin Wissel[a], Supratik Dasgupta[b], Alexander Benes[c,d], Roland Schoch[e], Matthias Bauer[e], Ralf Witte[d], Andrew Dominic Fortes[f], Emre Erdem[g], Jochen Rohrer[h], Oliver Clemens[a,d]*

[a] Technische Universität Darmstadt, Institut für Materialwissenschaft, Fachgebiet Materialdesign durch Synthese, Alarich-Weiss-Straße 2, 64287 Darmstadt, Germany

[b] Technische Universität Darmstadt, Institut für Materialwissenschaft, Fachgebiet Dünne Schichten, Alarich-Weiss-Straße 2, 64287 Darmstadt, Germany

[c] Techische Universität Darmstadt, Institut für Materialwissenschaft, Gemeinschaftslabor Nanomaterialien, Alarich-Weiss-Straße 2, 64287 Darmstadt, Germany

[d] Karlsruher Institut für Technologie, Institut für Nanotechnologie, Hermann-von-Helmholtz-Platz 1, 76344 Eggenstein-Leopoldshafen, Germany

[e] Department Chemie, Universität Paderborn, Warburger Straße 100, 33098 Paderborn, Germany

[f] ISIS Facility, Rutherford Appleton Laboratory, Harwell Science and Innovation Campus, Didcot, Oxfordshire OX11 0QX, United Kingdom

[g] Albert-Ludwigs-Universität Freiburg, Institut für Physikalische Chemie, Albertstraße 21, 79104 Freiburg, Germany

[h] Technische Universität Darmstadt, Institut für Materialwissenschaft, Fachgebiet Materialmodellierung, Otto-Berndt-Straße 3, 64287 Darmstadt, Germany

* Corresponding Author

Fax: +49 6151 16 20965

E-Mail: oliver.clemens@md.tu-darmstadt.de

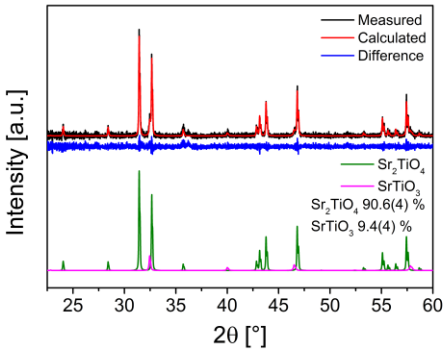

(a)

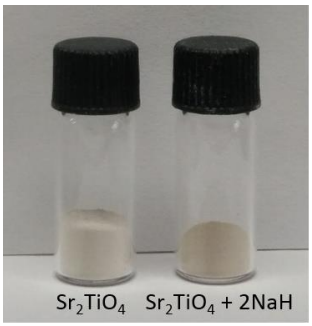

(b)

Figure S 1: (a) X-ray diffraction pattern and quantitative phase analysis of Sr_2TiO_4 + x NaH (x = 2) after the attempted reduction; (b) photograph of Sr_2TiO_4 and powder after reaction of Sr_2TiO_4 + x NaH (x = 2) showing no color change, which would indicate the formation of low valent titanium species.

Table S 1: Refined lattice parameters and quantitative analysis of Sr_2TiO_4, $Sr_2TiO_3F_2$ and reduction reaction products $Sr_2TiO_3F_2$ + x NaH *(0.25 ≤ x ≤ 3).*

	x in $Sr_2TiO_3F_2$ + x NaF	Phase	Space group	Weight Percent [%]	Lattice Parameters						
					a [Å]	b [Å]	c [Å]	α [°]	β [°]	γ [°]	Cell Volume [Å³]
Sr_2TiO_4		Sr_2TiO_4	*I4/mmm*	100.00	3.88479(8)		12.5943(4)				190.07(1)
$Sr_2TiO_3F_2$		$Sr_2TiO_3F_2$	*P4/nmm*	95.7(1)	3.8043(6)		15.509(5)				224.46(9)
		SrF_2	*Fm-3m*	4.4(1)							
$Sr_2TiO_3F_{2-x}$	0.25	$Sr_2TiO_3F_2$	*P4/nmm*	88.8(3)	3.807(1)		15.46(1)				224.0(2)
		intermediate phase 1	*P4/nmm*	2.4(1)	3.834(8)		14.19(5)				208.(1)
		intermediate phase 2	*I4/mmm*	18.0(8)	3.878(9)		12.67(7)				191.(1)
		NaF	*Fm-3m*	1.6(2)							
		SrF_2	*Fm-3m*	4.3(1)							
	0.5	$Sr_2TiO_3F_2$	*P4/nmm*	55.0(4)	3.811(2)		15.44(1)				224.2(3)
		intermediate phase 1	*P4/nmm*	2.6(1)	3.844(6)		14.19(5)				210.(1)
		intermediate phase 2	*I4/mmm*	32.6(5)	3.880(3)		12.64(2)				190.3(5)
		NaF	*Fm-3m*	4.9(2)							
		SrF_2	*Fm-3m*	4.0(1)							
	0.75	$Sr_2TiO_3F_2$	*P4/nmm*	12.5(3)	3.806(5)		15.40(4)				223.1(9)
		intermediate phase 1	*P4/nmm*	6.5(2)	3.89(1)		13.93(6)				210.(2)
		$Sr_2TiO_3FH_{0.48}$	*P-1*	67.8(4)	5.59(1)	5.54(1)	12.91(1)	90.48(1)	89.48 (2)	89.46(1)	399.4(1)
		NaF	*Fm-3m*	9.7(3)							
		SrF_2	*Fm-3m*	3.6(1)							
	1	$Sr_2TiO_3FH_{0.48}$	*P-1*	76.3(5)	5.571(5)	5.56(1)	12.907(2)	91.25(2)	89.351(10)	89.564(6)	396.5(1)
		intermediate phase 1	*P4/nmm*	6.3(5)	3.90(2)		13.79(9)				210.(3)
		NaF	*Fm-3m*	14.4(3)							
		SrF_2	*Fm-3m*	2.94(8)							
	1.25	$Sr_2TiO_3FH_{0.48}$	*P-1*	39.9(4)	5.5795(10)	5.52(1)	13.025(3)	90.75(2)	89.42(2)	89.39(1)	400.8(10)

	$Sr_2TiO_3H_{1.48}$	I4/mmm	41.1(4)	3.914(2)		12.69(4)				194.4(6)
	NaF	*Fm*-3*m*	16.1(3)							
	SrF_2	*Fm*-3*m*	2.9(1)							
1.5	$Sr_2TiO_3FH_{0.48}$	*P*-1	33.0(7)	5.5931(19)	5.54(2)	12.917(5)	91.3(3)	90.0(15)	89.9(9)	400.06(4)
	$Sr_2TiO_3H_{1.48}$	I4/mmm	43.6(7)	3.909(3)		12.70(5)				194.1(8)
	NaF	*Fm*-3*m*	20.1(5)							
	SrF_2	*Fm*-3*m*	3.3(1)							
1.75	$Sr_2TiO_3FH_{0.48}$	*P*-1	21.1(5)	5.585(7)	5.54(1)	12.920(19)	90.83(15)	90.83(15)	89.73(18)	399.7(11)
	$Sr_2TiO_3H_{1.48}$	*I4/mmm*	54.0(5)	3.909(2)		12.70(3)				194.0(5)
	NaF	*Fm*-3*m*	21.1(4)							
	SrF_2	*Fm*-3*m*	3.0(1)							
2	$Sr_2TiO_3H_{1.48}$	*I4/mmm*	71.9(1)	3.9100(1)		12.722(1)				194.5(2)
	NaF	*Fm*-3*m*	22.5(3)							
	$NaF_{1-z}H_z$	*Fm*-3*m*	4.4(1)							
	SrF_2	*Fm*-3*m*	1.2(1)							
2.5 (excess NaH)	$Sr_2TiO_3H_{1.48}$	*I4/mmm*	67.0(6)	3.900(3)		12.75(3)				193.9(5)
	NaF	*Fm*-3*m*	14.3(4)							
	$NaF_{1-z}H_z$	*Fm*-3*m*	15.8(6)							
	SrF_2	*Fm*-3*m*	3.0(1)							
3 (excess NaH)	$Sr_2TiO_3H_{1.48}$	*I4/mmm*	60.8(9)	3.907(2)		13.01(3)				198.5(5)
	NaF	*Fm*-3*m*	14.4(6)							
	$NaF_{1-z}H_z$	*Fm*-3*m*	16.3(9)							
	SrF_2	*Fm*-3*m*	1.0(2)							

Scanning Electron Microscopy Study

Scanning electron microcopy (SEM) images were recorded with a Philips XL30 FEG secondary electron microscope at a voltage of 30 kV.

(a) 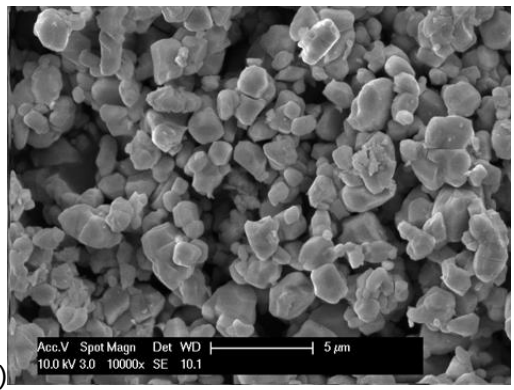

(b) 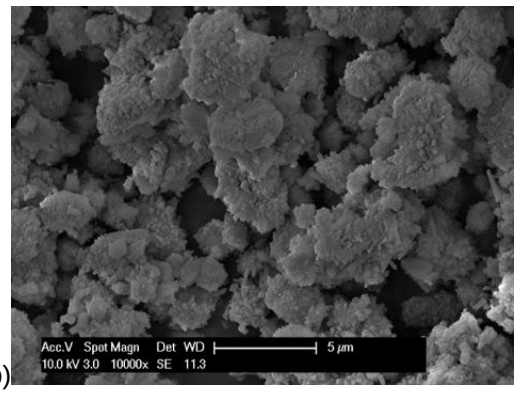

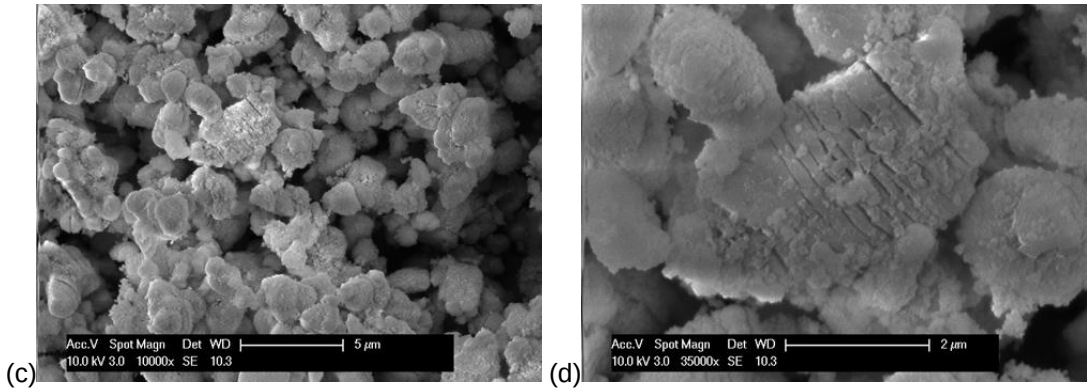

Figure S 2: SEM images of $Sr_2TiO_3F_2$ (a), unwashed $Sr_2TiO_3H_{1.48}$ with rough porous layer of NaF on top of particles (b), and washed Sr_2TiO_3 showing a layer-like breaking of particles (c and d).

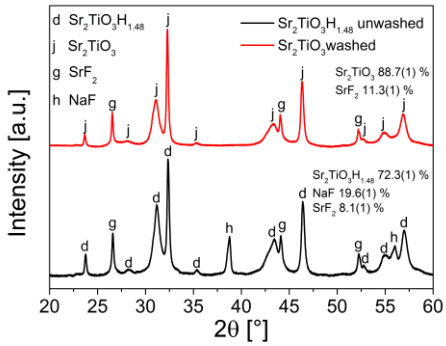

Figure S 3: X-ray diffraction patterns and quantitative phase analysis of reduction reaction product $Sr_2TiO_3F_2$ + x NaH (x = 2) before and after removal of NaF byproduct by washing with 0.25 M NH_4Cl in methanol.

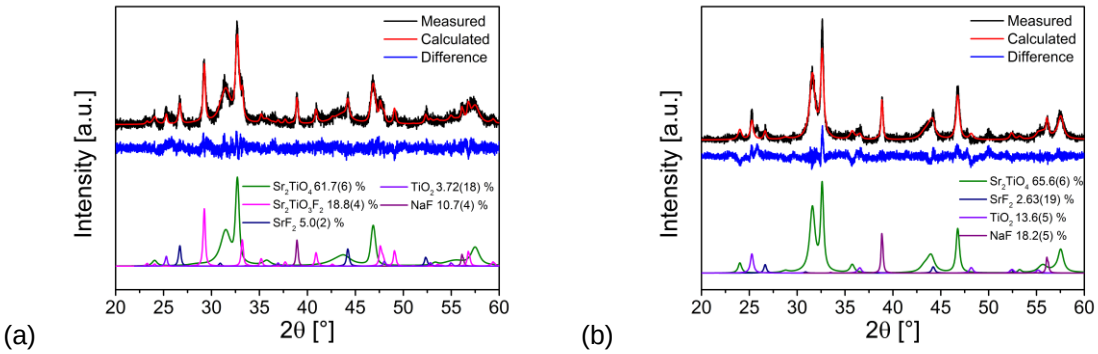

Figure S 4: (a) X-ray diffraction pattern and quantitative phase analysis of re-oxidized $Sr_2TiO_3FH_{0.48}$ (x=1); (b) X-ray diffraction pattern and quantitative phase analysis of re-oxidized $Sr_2TiO_3H_{1.48}$ (x=2).

Electron Paramagnetic Resonance

X-band (9.86 GHz) EPR measurements were performed by a BRUKER EMX spectrometer with the aid of a rectangular TE102 resonator from Bruker. The offset in the magnetic field and the exact g-factors in X-band measurements were determined with a polycrystalline DPPH (2-diphenyl-1-picrylhydrazyl) reference sample of well-known g-factor (g = 2.0036). The EPR spectral analysis has been performed using the WINEPR program from Bruker. The following EPR experimental parameters were used: microwave power: 1 mW; modulation amplitude: 2 G; time constant: 163.84 ms; receiver gain: 2×10^4. To determine EPR signal quantitatively we employed a spin counting procedure as described previously [1-2].

Room temperature X-band EPR measurements of $Sr_2TiO_3F_2$, as well as of $Sr_2TiO_3FH_{0.48}$ and $Sr_2TiO_3H_{1.48}$ are shown in Figure S 5 a. EPR measurements are very sensitive to the presence of paramagnetic species, such as electronic charge carriers on Ti^{3+} (Ti^{4+} and Ti^{2+} are EPR inactive), and / or electronic charge carriers located on anion vacancies. Therefore, as expected, no signal is observed for the diamagnetic $Sr_2TiO_3F_2$. On the other hand, for $Sr_2TiO_3FH_{0.48}$ and $Sr_2TiO_3H_{1.48}$, EPR signals could be detected and indicate the presence of unpaired electrons at ambient temperature, as would be expected for Ti^{3+}. For both samples, different paramagnetic species are indicated by two strong EPR active signals (a broad Gaussian line and a sharp line with overlapping EPR centers). The g-values for both sharp signals are in the order of 2.0, which agrees well with what has been previously reported for Ti^{3+} species [3-5]. The fact that more than one EPR signal has been observed could be explained by different degrees of structural disorder in the compound, e.g. more or less direct neighbours of Ti^{3+} species. Broader signals were also found for other Ti compounds, where it was explained by distortions of the local octahedron to lower symmetry and/or distribution of local structural distortions around the active center. Overall, the presence of different signals with different width is in agreement with the fact that $Sr_2TiO_3FH_{0.48}$ and $Sr_2TiO_3H_{1.48}$ show strong degrees of structural disorder which must result in different local configurations, and which would result in a distribution of signals around some mean average.

The intensity of the EPR signal of Ti^{3+} signal is strongly dependent on temperature, and low temperatures are often required to be even able to detect this species [6-7]. By integrating the first derivative of the EPR signal, one can obtain the concentration of the EPR centers, which are active at ambient temperature (Figure S 5 b and c, 1.7×10^{18} spins/g and 2.9×10^{17} spins/g for $Sr_2TiO_3H_{1.48}$ and $Sr_2TiO_3H_{0.48}$, respectively). In agreement with the previous literature on topochemically reduced titanates [8] (which to the best of our knowledge did not evaluate the EPR signal quantitatively and but only qualitatively), the overall amount of Ti^{3+} and/or free electrons in the sample at ambient temperature given in the article is therefore based on the evaluation of the magnetic data and the compositional analysis.

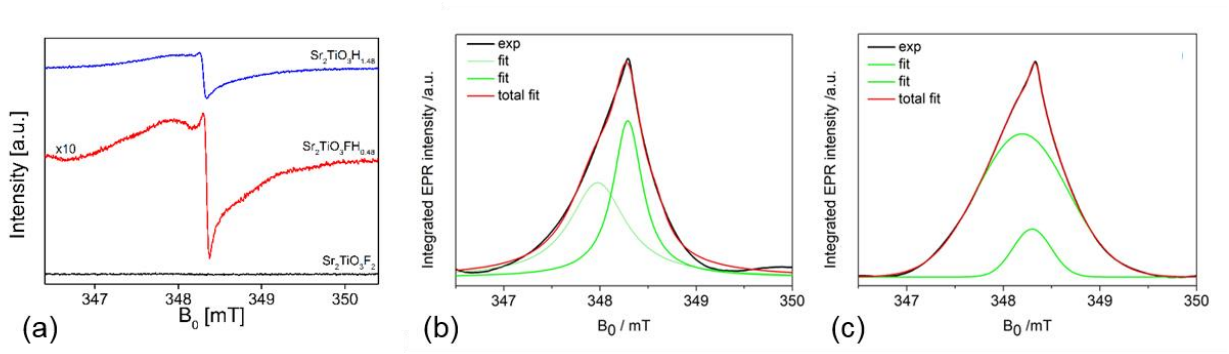

Figure S 5: (a) Room temperature X-band EPR spectra of $Sr_2TiO_3F_2$, $Sr_2TiO_3FH_{0.48}$ and $Sr_2TiO_3H_{1.48}$; *(b) Quantification of the Ti^{3+} species, which are EPR active at room temperature* of $Sr_2TiO_3FH_{0.48}$; *(c) Quantification of the Ti^{3+} species, which are EPR active at room temperature of $Sr_2TiO_3H_{1.48}$.*

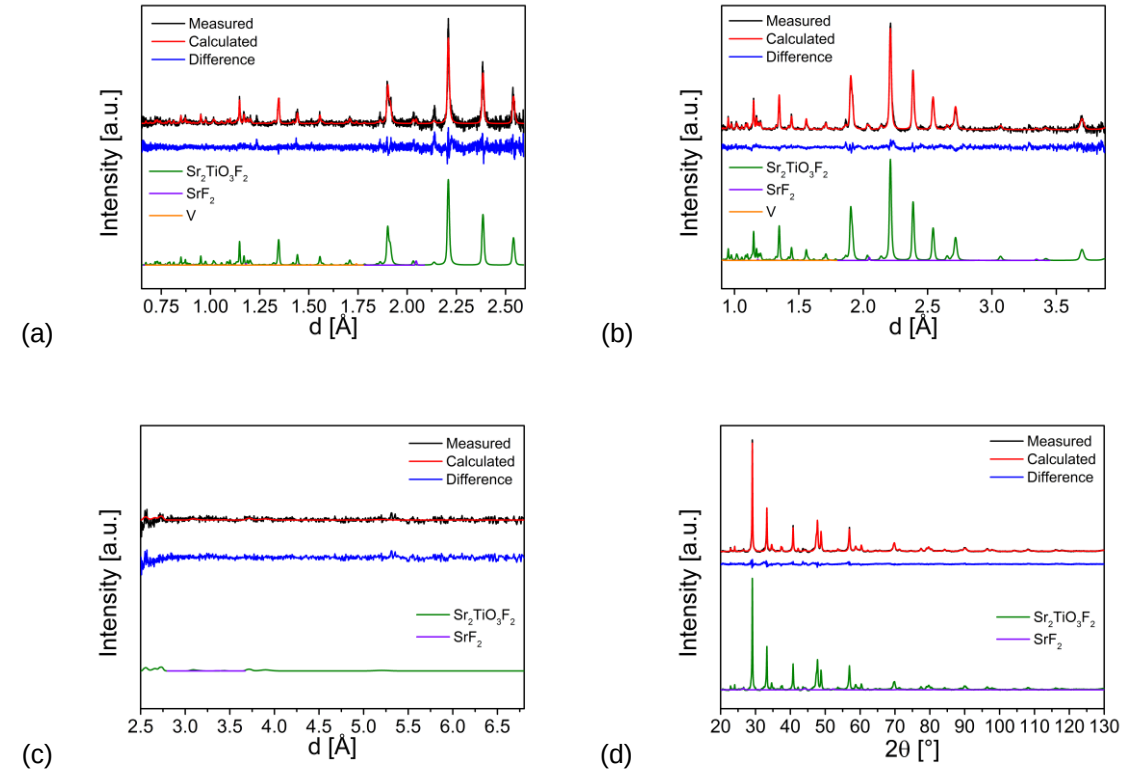

Figure S 6: Coupled Rietveld analysis of $Sr_2TiO_3F_2$ (space group: *P4/nmm*) of HRPD bank 1 data (a), HRPD bank 2 data (b), HRPD bank 3 data (c),and XRD data (d).

Table S 2: Structural parameters for $Sr_2TiO_3F_2$ (space group: P4/nmm) from coupled Rietveld analysis of XRD and NPD data.

Atom	**Wyckoff site**	**x**	**y**	**z**	**Occupancy**
Sr1	2c	**3/4**	**3/4**	0.0976(1)	**1**
Sr2	2c	**3/4**	**3/4**	0.3949(1)	**1**
Ti	2c	**1/4**	**1/4**	0.2584(2)	**1**
O1	4*f*	**1/4**	**3/4**	0.2861(2)	**1**
O2	2c	**1/4**	**1/4**	0.1579(3)	**1**
F1	2c	**1/4**	**1/4**	0.4444(1)	**1**
F2	2a	**1/4**	**3/4**	**0**	1.03(1)
***a* [Å]**	3.7929(1)		*c* [Å]	15.463(2)	
***R_{wp}* (XRD+NPD) [%]**	2.50	***GOF***	2.43	R_{Bragg} [%]	0.94 (XRD) 1.50 (NPD, bank 2)

Extended X-ray Absorption Fine Structure

The accuracy of the determined distances is 1 %, of the Debye-Waller-like factor 10 % and of the coordination numbers depending of the distance 10 % in case of distances shorter than 2.5 Å and -20 % for larger distances [9]. Initial fitting values for coordination numbers and distances were adopted from Rietveld-analysis and afterwards iterated freely in every fit as well as the Debye-Waller-like factor and the amplitude-reducing factor.

For the fitting procedure a χ(k)-range from 3 to 11 was used for every substance. The χ(k) spectra are shown in Figure S 7.

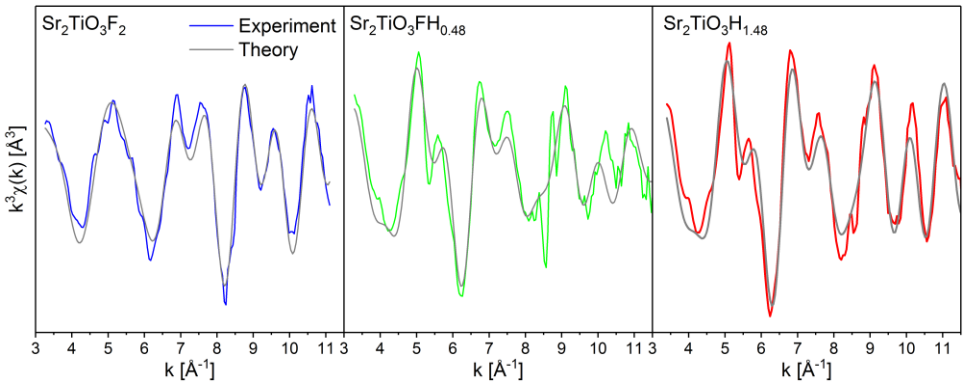

Figure S 7: χ(k) spectra of $Sr_2TiO_3F_2$ (left), $Sr_2TiO_3FH_{0.48}$ (middle) and $Sr_2TiO_3H_{1.48}$ (right).

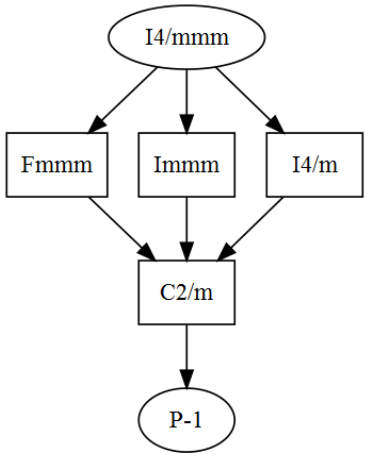

Figure S 8: Symmetry tree (http://www.cryst.ehu.es/cgi-bin/cryst/programs/nph-show_graph) for a series of translationengleiche symmetry lowerings to triclinic, which maintain translational symmetry.

Table S 3: Comparison of different structural distortion models for the analysis of powder diffraction data.

$(100)_{I4/mmm}$ **NPD, bank 1**	**$(220)_{I4/mmm}$ at 1.39 Å / $(206)_{I4/mmm}$ at 1.46 Å** **NPD, bank 1**	**$(200)_{I4/mmm}$** **XRD**	
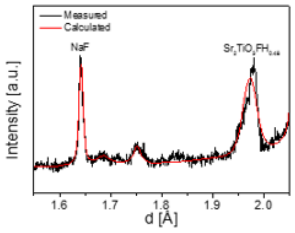	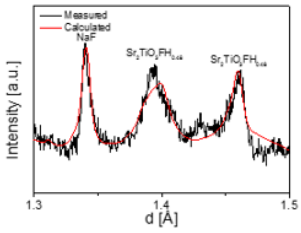	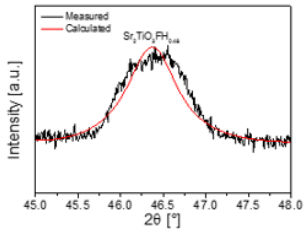	Tetragonal R_{wp} (XRD+NPD) = 3.55 %
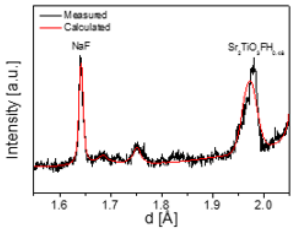	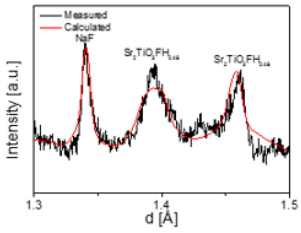	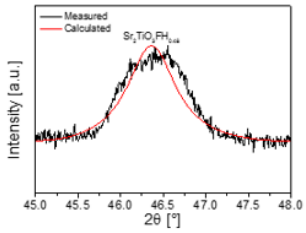	Orthorhombic R_{wp} (XRD+NPD) = 3.51 %
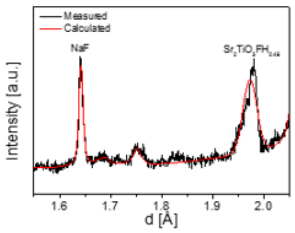	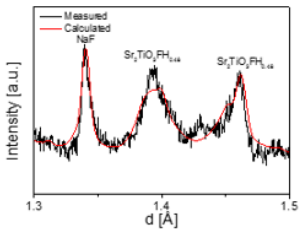	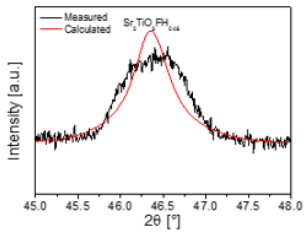	Monoclinic (α ≠ 90°) R_{wp} (XRD+NPD) = 3.36 %
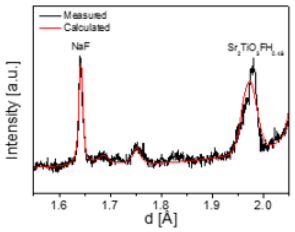	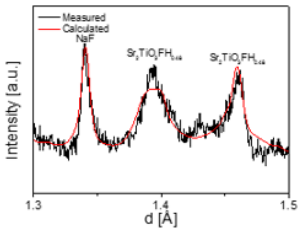	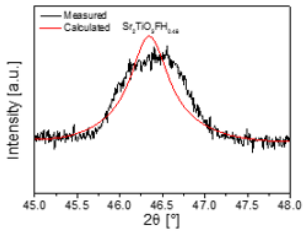	Monoclinic (β ≠ 90°) R_{wp} (XRD+NPD) = 3.43 %
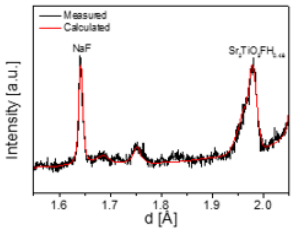	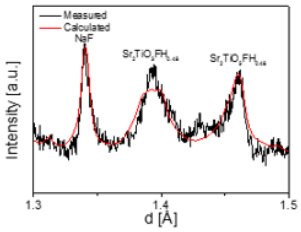	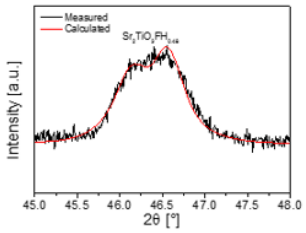	Monoclinic (γ ≠ 90°) R_{wp} (XRD+NPD) = 3.24 %
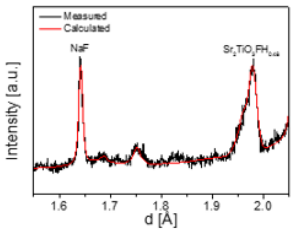	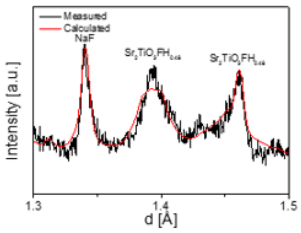	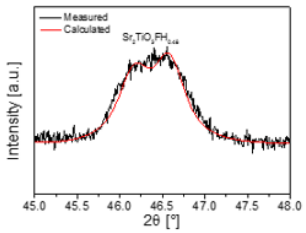	Triclinic R_{wp} (XRD+NPD) = 3.10 %

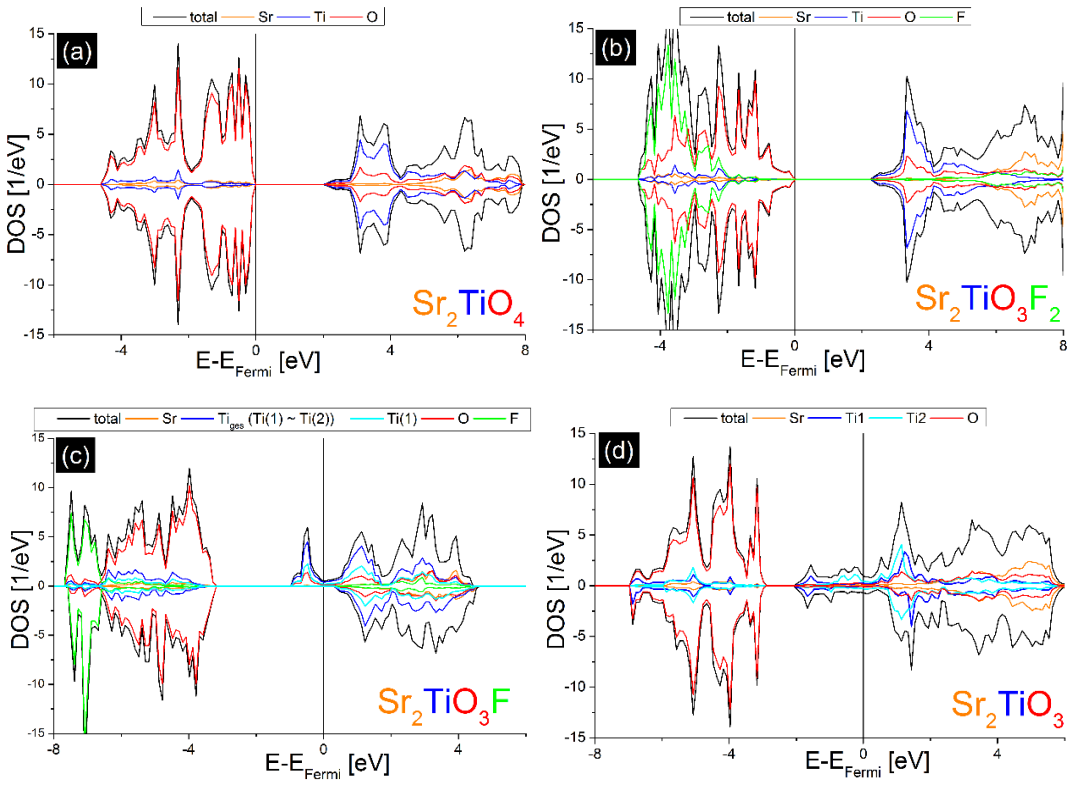

Figure S 9: DOS and pDOS of Sr_2TiO_4 (a), $Sr_2TiO_3F_2$ (b), Sr_2TiO_3F (c), and Sr_2TiO_3 (d). The DOS are shown for the for the most stable configurations of the anion lattice with U_{eff} = 2 eV.

Table S 4 Calculated reaction enthalpies and free reaction enthalpies from energies of optimized structures calculated by the DFT+U method considering the formation of H_2O and HF. The entropic contributions were calculated from the standard formation entropy of hydrogen, H_2O and HF at the reaction temperature of 573 K [10]

Reaction equation	ΔH [eV] < 0 → exothermal > 0 → endothermal	-TΔS [eV] at T = 573 K = 300 °C [10] for gaseous species	ΔG [eV] < 0 → exergonic > 0 → endergonic
Sr_2TiO_4 + NaH → $Sr_2TiO_{3.5}$ + ½ Na_2O + ½ H_2(g)	+1.09	-0.45	+0.63
Sr_2TiO_4 + NaH → Sr_2TiO_3 + ½ Na_2O + ½ H_2O(g)	+2.31	-0.64	+1.67
$Sr_2TiO_3F_2$ + NaH → Sr_2TiO_3F + NaF + ½ H_2(g)	+0.10	-0.45	-0.35
$Sr_2TiO_3F_2$ + NaH → Sr_2TiO_3 + NaF + HF(g)	+2.72	-1.07	+1.65

References

1. Parashar, S. K. S.; Murty, B. S.; Repp, S.; Weber, S.; Erdem, E., Investigation of intrinsic defects in core-shell structured ZnO nanocrystals. *Journal of Applied Physics* **2012,** *111* (11), 113712.
2. Schneider, J. J.; Hoffmann, R. C.; Engstler, J.; Dilfer, S.; Klyszcz, A.; Erdem, E.; Jakes, P.; Eichel, R. A., Zinc oxide derived from single source precursor chemistry under chimie douce conditions: formation pathway, defect chemistry and possible applications in thin film printing. *Journal of Materials Chemistry* **2009,** *19* (10), 1449-1457.
3. Laguta, V. V.; Glinchuk, M. D.; Kuzian, R. O.; Nokhrin, S. N.; Bykov, I. P.; Jastrabik, L.; Rosa, J., Electron Spin Resonance of Ti^{3+} in $KTa_{0.9}Nb_{0.1}O_3$. *Solid State Commun.* **2002,** *122*, 277-281.
4. Xiong, L.-B.; Li, J.-L.; Yang, B.; Yu, Y., Ti^{3+} in the Surface of Titanium Dioxide: Generation, Properties and Photocatalytic Application. *Journal of Nanomaterials* **2012,** *2012*, 1-13.
5. Xin, X.; Xu, T.; Wang, L.; Wang, C., Ti^{3+}-self doped brookite TiO_2 single-crystalline nanosheets with high solar absorption and excellent photocatalytic CO_2 reduction. *Sci Rep* **2016,** *6*, 23684.
6. Corradi, G.; Zaritskii, I. M.; Hofstaetter, A.; Polgar, K.; Rakitina, L. G., Ti3+ on Nb site: A paramagnetic Jahn-Teller center in vacuum-reduced LiNbO3:Mg:Ti single crystals. *Physical Review B* **1998,** *58* (13), 8329-8337.
7. ERDEM, E.; JAKES, P.; EICHEL, R.-A.; SINCLAIR, D. C.; PASHA, M.; REANEY, I. M., FORMATION OF $(Ti_{Ti}^{'} - V_O^{\bullet\bullet})^{\bullet}$ DEFECT DIPOLES IN BaTiO3 CERAMICS HEAT-TREATED UNDER REDUCED OXYGEN PARTIAL-PRESSURE. *Functional Materials Letters* **2010,** *03* (01), 65-68.
8. Poussacq, T.; Kabbour, H.; Colis, S.; Vezin, H.; Saitzek, S.; Gardoll, O.; Tassel, C.; Kageyama, H.; Robert, C. L.; Mentré, O., Reduction of $Ln_2Ti_2O_7$ Layered Perovskites: A Survey of the Anionic Lattice, Electronic Features, and Potentials. *Chemistry of Materials* **2017,** *29* (3), 1047-1057.
9. Bauer, M.; Bertagnolli, H., X-Ray Absorption Spectroscopy – the Method and Its Applications. Schäfer, P. R.; Schmidt, P. P. C., Eds. Wiley-VCH Weinheim, 2012; pp 231-270.
10. Chase Jr., M. W., NIST-JANAF Thermochemical Tables, Fourth Edition, Monograph 9 (Part I and Part II). *Journal of Physical and Chemical Reference Data* **1998**.